Proceedings of the 13th UK Automatic Control Council (UKACC) International Conference on Control (CONTROL2022), 20-22 April 2022, Plymouth, UK. DOI:10.1109/Control55989.2022.9781449

Control of an eVTOL using Non-linear Dynamic Inversion

Emmanuel Enenakpogbe, James F. Whidborne, Linghai Lu
Centre for Aeronautics
School of Aerospace, Transport and Manufacturing
Cranfield University
Bedfordshire, United Kingdom

***Abstract*—This paper presents a non-linear dynamic inversion based flight controller using virtual controls, generalised forces and moments for the longitudinal motion control of a VTOL aircraft including transition manoeuvres. The control architecture is general for piloted, semi-automatic and fully-automated flight. It consists of a main inner-loop NDI controller that is used for forward cruise flight and an outer linear controller used for low speed and hover. Forward and backward transition manoeuvres are executed by switching between the NDI-based controller and position control loops. Simulation results show the control potential for both hover and cruise as well as over the vital transition flight phase.**

***Index Terms*—NDI, Transition, UAM, Longitudinal, Full Envelop, easy-to-fly, virtual controls, VTOL, generalized moments and forces, angle-of-attack, high level motion controller, virtual controller**

I. Introduction

There is a need for new urban transport solutions to overcome the problems of congestion and pollution in the ever-growing major urban conurbations. The concept of Urban Air Mobility (UAM) has been proposed to address this problem [1]. Fixed wing aircraft technologies, despite being mature and reliable, have many constraints, both infrastructural and operational, that limit their applicable for UAM. Piloted all-electric vertical takeoff and landing (eVTOL) 'air taxis' (also known as flying cars) which could leapfrog and cruise at 180 mph at altitudes of around 1,000 ft to 2,000 ft, have been identified as a promising solution because when widely commercialized, will usher in a nimble form of intracity travel, transporting people on the shortest possible route between two locations [2].

However eVTOLs will require fly-by-wire augmented flight control systems that not only satisfy the primary flight objective of safety-of-flight (stability, envelope protection, fault tolerance, robustness to both external and internal disturbances etc.) and the secondary objectives (flight performance, efficiency, drag reduction, flying and handling qualities etc.), but also provide a high degree of automation to reduce the cost of pilot training. Furthermore, eVTOL aircraft need a wide range of operating modes (hover, forward flight, transition—including post-stall operation, cruise, climb, descent, etc.). One of the trends in EVTOL development is towards finding a unified-control approach valid in all flight modes without the need to switch among flight controllers or to perform predefined-gain scheduling, in order to address the challenge of a need to mitigate control complexity and available computing resources [3], [4]. A pre-requisite for eVTOL "air-taxis" business model is to have an aircraft that is relatively "easy" to fly requiring minimal pilot training compared to that of commercial and military aircraft hence one aim of this work is to get a controller structure/architecture which is general for piloted, semi-automatic and automated flight. Non-linear control schemes which can handle the non-linearities offer potential solutions in providing a unified-control approach valid in all flight modes to perform predefined-gain scheduling. Nonlinear Dynamic Inversion (NDI) is a well-established Non-linear control approach which has been widely applied in various forms [5]–[14]. Although NDI can deal with the non-linearities in the motion of an aircraft, a drawback is its poor performance in the presence of external disturbances and model uncertainties because it relies on an accurate model of the controlled system. Hence NDI should be combined with a robust controller to deal with these disturbances and uncertainties [15], [16].

In order to ensure the required [17]–[19] levels of reliability, safety and fault tolerance in the emerging UAM industry, VTOLs are overactuated, i.e. equipped with more effectors than the degrees of freedom they control, thus introducing redundancy in case of effector failure. This over-actuation creates the challenge of allocation of overall control demand to individual redundant effectors which is known as control allocation.

Lombaerts et al [20] initially applied NDI for the integrated attitude/altitude control of a quadrotor eVTOL vehicle only for hover, low forward speed and attitude control but later [21] applied NDI for the full envelop control of a quadrotor eVTOL vehicle using a Unified Framework with the control architecture consisting of several flight control modes requiring switching between them. In this paper, a simple control (fewer flight control modes and less switching between modes) architecture and easy-to-fly full envelope flight control for a generic eVTOL vehicle model but with focus only on the longitudinal motion in order to demonstrate the effectiveness of the approach. The flight envelope of the proposed NDI control includes cruise-speed flight as well as low-speed and

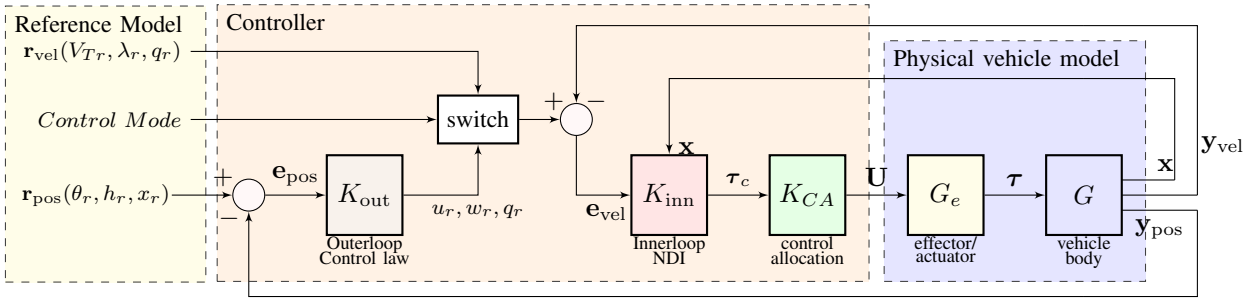

Fig. 1: Control Architecture

hover, and importantly, the transition between these flight regimes. A complete motion (including lateral-directional motion) controller using this control approach will be the subject of a future publication. The actuation is not considered, the approach utilizes a 'virtual' or 'desired' control. This is a common approach for NDI and requires subsequent design of a control allocation scheme [22], [23]. Note that the control allocation part of problem and flying and handling qualities consideration (part of the reference model functionality) are not addressed in this paper.

In the next section, the model (a generic VTOL model) is outlined and the longitudinal motion equations of motion are given. In Section III, the control framework and architecture are presented. Two control loops are defined, an inner loop for velocity control and an outer-loop for position control, a switch is added so that either velocity or position are the reference demands. The simulations results of some selected manoeuvres are presented and analysed in Section IV. In the final section, the proposed scheme is discussed as well as the limitations and implementation problems and the future work.

II. Vehicle Dynamic Model

The vehicle model is a representative aircraft model of a generic VTOL Air Vehicle.

The Vertical Flight Society (VFS) has categorized eVTOLs into the following [24], [25]:

- Vectored Thrust (including tilt-wing and tilt-rotor)
- Lift + Cruise
- Wingless
- Hover Bikes
- Electric Helicopters

Vectored Thrust eVTOLs are supported in vertical takeoff and landing flight by the horizontally-mounted propulsion systems, directing thrust downwards to generate lift. Horizontal flight is supported primarily by lift generated from the wings, with some or all of the propulsion systems rotated to the required position to provide horizontal thrust for forward speed. Tilt-wings are a challenging configuration for control, particularly in the transition phase between hover and cruise, where the aerodynamics may be in a post-stall condition. This is the configuration considered in this paper. An example of an aircraft in the class is the Airbus A^3 Vahana [26].

Consider an air vehicle with 3-degrees of freedom, pitch, heave and surge, which represent the longitudinal motion. The equations of motion are given by:

$$\dot{x} = u\cos\theta + w\sin\theta \tag{1}$$
$$\dot{z} = w\cos\theta - u\sin\theta \tag{2}$$
$$\dot{\theta} = q \tag{3}$$
$$\dot{u} = \tfrac{1}{m}(X + T_X) - g\sin\theta - qw \tag{4}$$
$$\dot{w} = \tfrac{1}{m}(Z + T_Z) + g\cos\theta + qu \tag{5}$$
$$\dot{q} = \tfrac{1}{I_{yy}}(M_a + M_y) \tag{6}$$

where x is the distance in the earth horizontal axis, u is the body axis horizontal velocity, θ is the pitch angle, w is the body axis vertical down velocity, q is the pitch rate, z is the earth vertical down axis distance, m is the vehicle mass, X is the net aerodynamic force acting at the centre of gravity in the body x-direction, T_X is the rotor thrust in the body x-direction, g is the gravitational acceleration constant, Z is the net aerodynamic force in the body z-direction, T_Z is the rotor thrust in the body z-direction, I_{yy} is the moment of inertia about the y-body direction, M_a is the net aerodynamic moment acting about the body y-direction, and M_T is the rotor moment acting about the body y-direction.

The aerodynamic terms X, Z and M_a are dependent upon the airspeed and wing angles of attack and include post-stall aerodynamics developed by [27]. The aerodynamic prediction method models the boundary layer separation due to stall using an effective decambering on each wing section. The aerodynamics of the configuration is rapidly calculated using superposition of stored lift distributions, which allows the method to be used in real-time flight simulation even for post-stall conditions. Space constraints preclude further description here.

The longitudinal state variable vector $\mathbf{x}$ and virtual control vector $\boldsymbol{\tau}$ are respectively given by:

$$\mathbf{x} = \begin{bmatrix}\theta & q & x & z & u & w\end{bmatrix}^T \tag{7}$$
$$\boldsymbol{\tau} = \begin{bmatrix}T_X & T_Z & M_y\end{bmatrix}^T \tag{8}$$

III. Control Design

A. Control Architecture

The controller structure/architecture is general for piloted, semi-automatic and automated flight. The system consists of a

reference model, a controller and the physical vehicle model. The reference model performs reference input computation, scaling and limitation (e.g. flight envelope protection), flight mode selection (automode or manual mode), control mode switching and pilot command filtering for flying and handling qualities compliance. This paper does not cover the reference model functionalities.

The architecture is shown in Figure 1. The controller comprises a high-level motion controller and the control allocation. The higher-level motion controller consists of an outer-loop position controller and an inner loop velocity controller. A hard switch is used to switch between velocity and position control. In velocity control mode the references are airspeed V_T, flight path angle λ, and pitch rate q. These are controlled directly by the NDI inner-loop feedback. For position control mode, the references are lateral position x, altitude h and pitch attitude, θ.

The physical vehicle model consists of an effector/actuator model, thus normally would include low-level actuator controller (e.g. servo controllers), and the physical model with virtual controls. For the remainder of the work, it is assumed that a perfect control allocation scheme is in operation, so that the virtual control demands output, $\boldsymbol{\tau}_c$, that is produced by the inner-loop controller, K_{inn} is equal to the forces and moments vector, $\boldsymbol{\tau}$, that characterizes the physical model give by (8).

B. NDI Controller Problem formulation

Based on the exposition in [28], in this section the NDI approach is outlined. Consider a plant model with general state equations given by:

$$\dot{\mathbf{x}} = f(\mathbf{x}) + g(\mathbf{x})\mathbf{u} \tag{9}$$
$$\mathbf{y} = h(\mathbf{x}) \tag{10}$$

where $\mathbf{x}(t) \in \mathbb{R}^n$ is the vector of state variables, $\mathbf{u} \in \mathbb{R}^m$ is the (virtual) control and $\mathbf{y}(t) \in \mathbb{R}^m$ is the vector of outputs to be controlled.

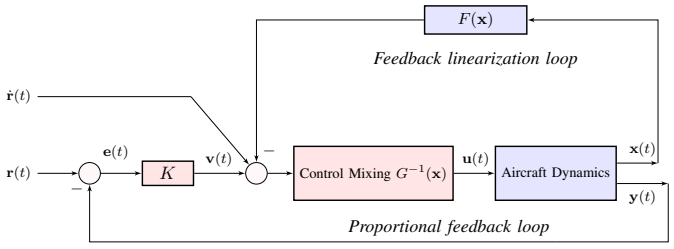

Fig. 2: NonLinear Dynamic Inversion (NDI) problem formulation

The error is given by:

$$\mathbf{e}(t) = \mathbf{r}(t) - \mathbf{y}(t) \tag{11}$$

where $\mathbf{r}(t) \in \mathbb{R}^m$ is the vector of reference signals to be tracked. Differentiating the output gives

$$\dot{\mathbf{y}} = \frac{\partial h}{\partial \mathbf{x}}\dot{\mathbf{x}} \tag{12}$$
$$= \frac{\partial h}{\partial \mathbf{x}} f(\mathbf{x}) + \frac{\partial h}{\partial \mathbf{x}} g(\mathbf{x})\mathbf{u} \tag{13}$$

Defining

$$F(\mathbf{x}) := \frac{\partial h}{\partial \mathbf{x}} f(\mathbf{x}), \qquad G(\mathbf{x}) := \frac{\partial h}{\partial \mathbf{x}} g(\mathbf{x}) \tag{14}$$

we get

$$\dot{\mathbf{y}} = F(\mathbf{x}) + G(\mathbf{x})\mathbf{u} \tag{15}$$

Rearranging, assuming that the function matrix $G(\mathbf{x})$ is always nonsingular, we get the control input to be

$$\mathbf{u} = G^{-1}(\mathbf{x})\left[-F(\mathbf{x}) + \dot{r} + \mathbf{v}\right] \tag{16}$$

where $\mathbf{v}$ is the output of the outer loop linear controller such that $\mathbf{v} = K\mathbf{e}$ if the controller is a proportional gain matrix, $K \in \mathbb{R}^{m\times m}$. Substituting for $\mathbf{u}$ in (13) gives

$$\dot{\mathbf{y}} = \frac{\partial h}{\partial \mathbf{x}} f(\mathbf{x}) + \frac{\partial h}{\partial \mathbf{x}} g(\mathbf{x}) G^{-1}(\mathbf{x})\left[-F(\mathbf{x}) + \dot{\mathbf{r}} + \mathbf{v}\right] \tag{17}$$
$$= F(\mathbf{x}) + G(\mathbf{x})G^{-1}(\mathbf{x})\left[-F(\mathbf{x}) + \dot{\mathbf{r}} + \mathbf{v}\right] \tag{18}$$
$$= \dot{\mathbf{r}} + \mathbf{v} \tag{19}$$

From (11), the error dynamics is given by:

$$\dot{\mathbf{e}} = \dot{\mathbf{r}} - \dot{\mathbf{y}} \tag{20}$$
$$= -\mathbf{v} \tag{21}$$

This is a first order system, so any linear control technique can be used to choose K to stabilize the error so that $\dot{\mathbf{e}} = -K\mathbf{e}$. Thus the total controller is

$$\mathbf{v} = K\mathbf{e} \tag{22}$$
$$\mathbf{u} = G^{-1}(\mathbf{x})\left[-F(\mathbf{x}) + \dot{\mathbf{r}} + \mathbf{v}\right] \tag{23}$$

The controller structure is shown in Figure 2 and consists of the linear output feedback loop (22) and the state feedback linearisation loop (23) (which assumes all the states are observable). The feedback linearisation loop ensures that the system from $\mathbf{v}(t)$ to $\mathbf{y}(t)$ appears like a linear system with poles at the origin, thus simplifying the outer tracking loop design. The velocity feedforward term $\dot{r}$ improves the tracking accuracy of the closed-loop system. This signal is generated either by the pilot inceptor for manned operation or the guidance system for automated flight.

Since the controller in Figure 2 contains a model of the aircraft dynamics (14), the nonlinear functions of the aircraft must be known in order to implement it.

1) Zero Dynamics: Substituting the control input (23) into the state equations (9), the full closed-loop dynamics is given by:

$$\dot{\mathbf{x}} = \left[I - g(\mathbf{x})G^{-1}(\mathbf{x})\frac{\partial h}{\partial \mathbf{x}}\right] f(\mathbf{x}) + g(\mathbf{x})G^{-1}(\mathbf{x})\left[\dot{\mathbf{r}} + \mathbf{v}\right] \tag{24}$$

where I denotes the identity matrix. To ensure that the system is stable, the *zero dynamics* must be stable. The zero dynamics

is the dynamics of the system when the auxiliary input $\mathbf{v}(t)$ is selected to give an output $\mathbf{y}(t)$ equal to zero. Since $\mathbf{y}(t) = 0$, then $\dot{\mathbf{y}}(t) = 0$, such that $\mathbf{v}(t) = -\dot{\mathbf{r}}(t)$ which when substituted into (24) yields the *error dynamics* equation given by:

$$\dot{\mathbf{x}} = \left[I - g(\mathbf{x})G^{-1}(\mathbf{x})\frac{\partial h}{\partial \mathbf{x}} \right] f(\mathbf{x}) \tag{25}$$

2) Controlled Variables (CV): A necessary and sufficient condition for a successful NDI design is the selection of the *controlled variables (CV)* ($\mathbf{y} = h(\mathbf{x})$) that will make the *zero dynamics* stable. For this paper, the CV was tested for suitability on a linearized version of the error dynamics at a cruise conditions using MATLAB simulation to confirm that the *zero dynamics* state converge to zero from various initial conditions, as suggested by [28].

Since the state equations for $\dot{x}$, $\dot{z}$ and $\dot{\theta}$ have no control terms, they are referred to as *uncontrollable states* while the remaining longitudinal states $\dot{u}$, $\dot{w}$ and $\dot{q}$ are called *controllable states*[1]. Equations (1), (2) and (3) are called the *complimentary equations* and (4), (5) and (6) the *controlled equations* [29]. A simple rule is to ensure that the selected CV are at least a function of all the controllable states. For this paper, the selected CV, $\mathbf{y} = h(\mathbf{x})$ for the three (surge, heave and pitch) degrees of freedom are given by $\mathbf{y} = (u, w, q)^T$.

C. Outer-Loop Linear Controller

As stated in [29], to control the uncontrollable states, the controllable states can used as the controls resulting in a cascaded loop consisting of the inner controllable state variables (u, w, q) velocity loop and an outer uncontrollable state variables (x, z, θ) position loop. A simple diagional proportional (P) linear controller is used for the outer loop control.

The outer-loop linear controller consists of the following:

- Altitude ($h = -z$) controller - PI Controller
- Pitch attitude (θ) controller - P Controller
- Position (x) controller - PI Controller

Position control is used only for Hover and low ground speed control in the presence of external disturbances. The outer-loop controller parameters are provided in Table I.

D. Control Limitation and Flight Modes

The virtual controls, (T_X, T_Z, M_y) are limited to represent actuator limits for the real controls. The pilot command and control limits applied are listed in Table I.

The various flight regime modes are:

- *Vertical TakeOff and Landing (VTOL)*: w control, $u = 0$ hold, $q = 0$ hold
- *Short TakeOff and Landing (STOL)*: u control, w control, $q = 0$ hold
- *Climb, Descend, Approach and Flare (CDAF)*: u control, w control, $q = 0$ hold *or* u and w hold, θ control
- *Cruise*: w hold, u control, $q = 0$ hold
- *Hover*: x and z hold, $u = w = q = 0$ control, θ control
- *Forward Transition*: move from low-speed/hover flight to cruise/high-speed flight
- *Backward Trnsition*: move from cruise/high-speed flight to low-speed/hover flight

[1]As distinct from the *controllable modes*, an entirely different concept that derives from Kalman's well-known controllability test.

IV. Simulations Results

The vehicle model and NDI controller are coded in Simulink.[2] The constants used for the model are given in Table I. It is assumed that the measurements are noise-free.

TABLE I: Simulink simulation coefficients.

Total mass, m	7.5×10^2 kg
Gravitational constant, g	9.81 m s^{-2}
Air density, ρ	1.225 kg m^{-3}
Wing surface area, S	0.0165×10^3 m^2
Wing aerodynamic mean chord, $\bar{c}$	1.5 m
Wing span, b	11 m
Moment of inertia in the pitch axis, I_{yy}	2.839×10^3 kg m s^2
Inner loop NDI u tracking loop P gain, K_{up}	10 N m^{-1} s
Inner loop NDI w tracking loop P gain, K_{wp}	10 N m^{-1} s
Inner loop NDI q loop P gain, K_{qp}	10 N m rad^{-1} s
Outer loop altitude control P gain, K_{hp}	1 N m rad^{-1}
Outer loop altitude control integral gain, K_{hi}	0.2 N m rad^{-1}
Outer loop attitude control P gain, $K_{\theta p}$	1 N m rad^{-1}
Outer loop position hold loop P gain, K_{xp}	1 N m^{-1}
Outer Loop lateral position hold loop integral gain, K_{xi}	0.005 N m^{-1}
Pilot command filter time constant on (r_u, r_w)	0.25 s
Pilot command upper limit on r_u	$11g$ m s^{-1}
Pilot command lower limit on r_u	0 m s^{-1}
Pilot command upper limit on r_w	$0.8g$ m s^{-1}
Pilot command lower limit on r_w	$0.5g$ m s^{-1}
Pilot command limit on r_θ	$\pm\pi/10$ rad
Pilot commands filter time constant	0.25 s
Forward force control upper limit on T_x	1×10^5 N
Forward force control lower limit on T_x	0 N
Vertical force control upper limit on T_z	100×10^3 N
Vertical force control lower limit on T_z	10×10^3 N
Pitching moment control limit on M_y	

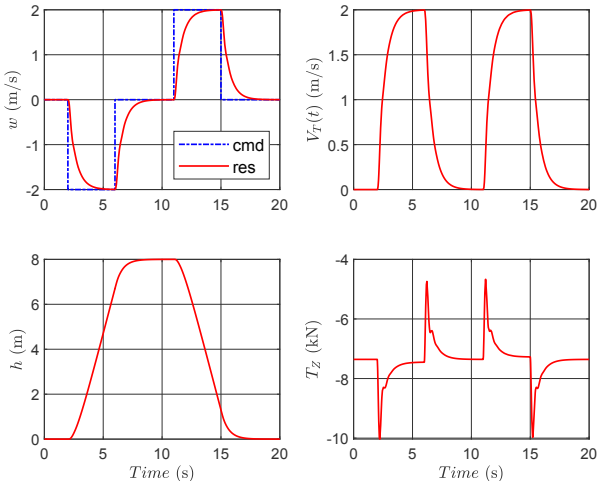

Fig. 3: Vertical Climb and Descent Manoeuvre

In order to evaluate the longitudinal control of the Generic EVTOL using virtual controls, four critical scenarios are investigated as follows:

[2]Data and MATLAB/Simulink simulation codes will be made available on the Cranfield University CORD repository doi:10.17862/cranfield.rd.xxxxxxx

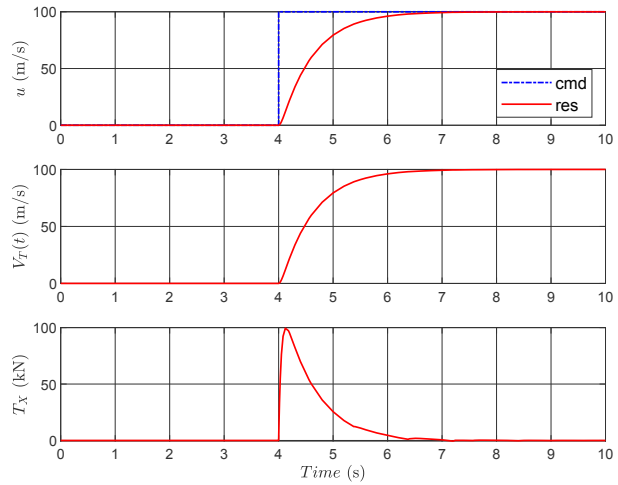

Fig. 4: Forward Transition Manoeuvre

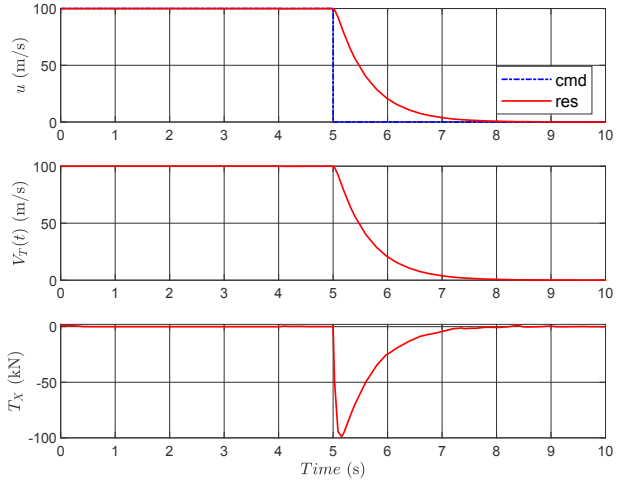

Fig. 5: Backward Transition Manoeuvre

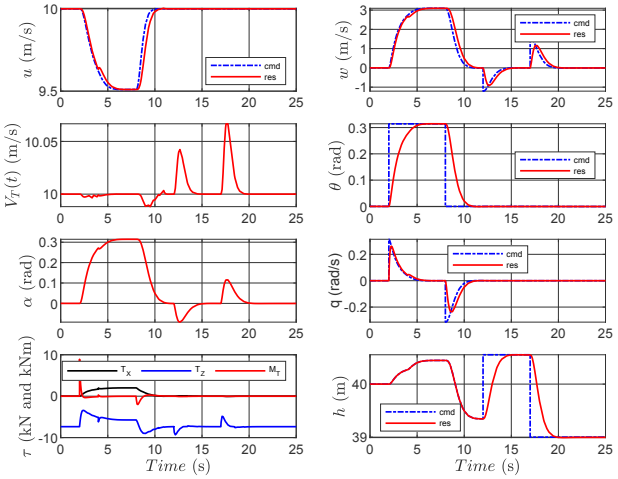

Fig. 6: Climb Descent Manoeuvre

a) Vertical Climb and Descent: : This manoeuvre starts at hover followed at time $t = 2$s by a constant rate vertical climb for 4s duration, then a constant altitude hover for 5s before a constant rate descent 4s duration to return the aircraft to the original position. At hover, the control mode changes

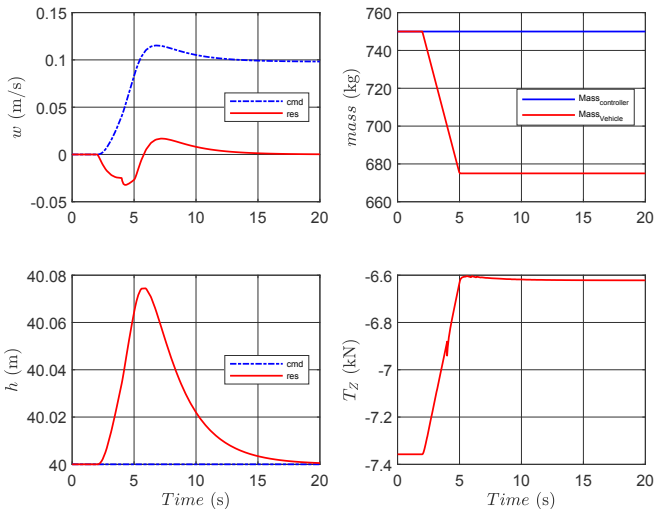

Fig. 7: Forward Flight Cruise Controller Robustness Test

from speed loop to position (low speed) control loop. The vertical airspeed, true airspeeds, altitude and virtual controls are shown in Figure 3. A hover (station keeping) logic switches to position control while absolute values of the commanded and actual speeds are less than a threshold. It can be seen that the controller performs well for the VTOL manoeuvre.

b) Forward Transition: : This manoeuvre starts with hover at 40m altitude with a forward speed change demand of 100 m/s at 4s. Thus this is a transition from low-speed hover to forward flight (cruise). The horizontal airspeed, true airspeeds and virtual controls are shown in Figure 4. The aircraft executes the transition in 1 s with negligible effect on the pitch and altitude. The horizontal thrust demand has a maximum of 20kN, but the maximum thrust slew rate is rather high.

c) Backward Transition: : This manoeuvre is a transition from 100m/s cruise trim condition (with constant 40 m altitude) to hover commencing at 5s. Thus this is a transition from forward flight (cruise) to low-speed (hover).The horizontal airspeed, true airspeeds and virtual controls are shown in Figure 5. The aircraft executes the transition in 1 s with negligible effect on the pitch and altitude.

d) Climb and Descent: : This test aims to demonstrate that the controller's outer and inner loops works correctly. Starting from zero pitch, constant 40m altitude, constant 10m/s forward speed,the following sequence of flight phase demands are executed: (1) command a pitch attitude of 18deg for 4s at time $t = 2$s while cruising at 10m/s (2) cancel (i.e. $r_\theta = 0\,\text{deg}$) the pitch attitude command 6s later and then turn on altitude control height hold (ACHH) 4s later for 3s (3) command a 4% altitude increase via Altitude Command (AC) for the next 4s (4) apply ACHH for 8s. The velocities, altitude, pitch attitude, pitch rate, angle of attack and virtual controls are shown in Figure 6. It can be seen that the virtual controller controls well in the pitch axis. Climb results from the increased angle of attack in phase (1) of the manoeuvre.

e) Forward Flight Robustness Test: : This test scenario serves to demonstrate the controller's robustness to model

parameter variation such as mass changes. In the case it tests the robustness of the altitude controller. It involves reducing the weight (simulating a fuel burn or load dump) of the vehicle during cruise while ACHH control mode is active. The vehicle was initialised at an altitude of 40m cruising at a horizontal speed of 10m/s. Then the mass of the vehicle was reduced by 10% from time t=2s to t=5s. The vertical airspeed, altitude and vehicle mass variation are shown in Figure 7. It can be seen that there was negligible variation in the vertical speed while the altitude initially increased by 0.25% but recovered within 15s of the mass reduction. In reality for an EVTOL, the centre of gravity (CG) and moment of inertia that is more likely to change due to its tilting mechanism.

V. Conclusions

The results demonstrates the ability of NDI to naturally handle VTOL's changes of a wide range of operating conditions (hover, forward flight and transition) removing the need for gain scheduling leading to improved levels of performance over conventional flight controller designs developed using linearizing approximations. The results demonstrate the tracking capabilities of the NDI scheme, and potentially the operational safety during transition when there may be high angles of attack. The pilot commands displayed on the plots are filtered commands. Note, however, that the saturation and slew-rate limitations (not shown) on virtual controls were intentionally set to high levels to reduce the effector/actuator limitations since the benefits of such limitations will not be achieve without real controls.

In order to test the full ability of the scheme, a control allocation scheme must be designed, which will automatically tilt the wings and apply variable thrust to effect the manoeuvres. This may introduce post-stall aerodynamic phases of flight, where the aerodynamic uncertainties will be more prevalent and unpredictable. The remains for future work whereby a complete longitudinal eVTOL control scheme with control allocation, effector model, real controls and actuator dynamics, as shown Figure 1, will be designed and tested. After successful desktop simulation, and design and test of the lateral dynamics controls, the model and controls will be implemented on the Cranfield University flight simulators and pilot-in-the-loop trials will be conducted to evaluate the handling qualities.

References

[1] "Uam vision concept of operations (conops) uam maturity level (uml) 4," https://ntrs.nasa.gov/citations/20205011091, [Accessed: 2021-11-06].

[2] R. W. Hascaryo and J. M. Merret, "Configuration-independent initial sizing method for uam/evtol vehicles," in *AIAA AVIATION 2020 FORUM*, 2020, p. 2630.

[3] G. J. Ducard and M. Allenspach, "Review of designs and flight control techniques of hybrid and convertible vtol uavs," *Aerospace Science and Technology*, vol. 118, p. 107035, 2021. [Online]. Available: https://www.sciencedirect.com/science/article/pii/S1270963821005459

[4] T. Lombaerts, J. Kaneshige, and M. Feary, "Control concepts for simplified vehicle operations of a quadrotor evtol vehicle," in *AIAA AVIATION 2020 FORUM*, 2020, p. 3189.

[5] S. H. Lane and R. F. Stengel, "Flight control design using non-linear inverse dynamics," *Automatica*, vol. 24, no. 4, pp. 471 – 483, 1988. [Online]. Available: http://www.sciencedirect.com/science/article/pii/0005109888900921

[6] P. Smith and A. Berry, "Flight test experience of a non-linear dynamic inversion control law on the vaac harrier," in *Atmospheric Flight Mechanics Conference*, 2000, p. 3914.

[7] P. Smith, "A simplified approach to nonlinear dynamic inversion based flight control," in *23rd Atmospheric Flight Mechanics Conference*, 1998, p. 4461.

[8] D. Ito, J. Georgie, J. Valasek, and D. T. Ward, "Reentry vehicle flight controls design guidelines: dynamic inversion," 2002.

[9] J. Georgie and J. Valasek, "Evaluation of longitudinal desired dynamics for dynamic-inversion controlled generic reentry vehicles," *Journal of guidance, control, and dynamics*, vol. 26, no. 5, pp. 811–819, 2003.

[10] J. Valasek and J. Georgie, "Selection of longitudinal desired dynamics for dynamic inversion controlled re-entry vehicles," in *AIAA guidance, navigation, and control conference and exhibit*, 2001, p. 4382.

[11] C. Miller, "Nonlinear dynamic inversion baseline control law: architecture and performance predictions," in *AIAA Guidance, Navigation, and Control Conference*, 2011, p. 6467.

[12] ——, "Nonlinear dynamic inversion baseline control law: flight-test results for the full-scale advanced systems testbed f/a-18 airplane," in *AIAA Guidance, Navigation, and Control Conference*, 2011, p. 6468.

[13] I. Gregory, "Modified dynamic inversion to control large flexible aircraft-what's going on?" in *Guidance, Navigation, and Control Conference and Exhibit*, 1999, p. 3998.

[14] P. Smith, *Functional control law design using exact non-linear dynamic inversion*. [Online]. Available: https://arc.aiaa.org/doi/abs/10.2514/6.1994-3516

[15] H. Yang and R. Morales, "Robust full-envelope flight control design for an evtol vehicle," in *AIAA Scitech 2021 Forum*, 2021, p. 0254.

[16] R. J. Adams, J. M. Buffington, and S. S. Banda, "Design of nonlinear control laws for high-angle-of-attack flight," *Journal of Guidance, Control, and Dynamics*, vol. 17, no. 4, pp. 737–746, 1994.

[17] J. Littell, "Challenges in vehicle safety and occupant protection for autonomous electric vertical take-off and landing (evtol) vehicles," in *AIAA Propulsion and Energy 2019 Forum*, 2019, p. 4504.

[18] A. Straubinger, R. Rothfeld, M. Shamiyeh, K.-D. Büchter, J. Kaiser, and K. O. Plötner, "An overview of current research and developments in urban air mobility–setting the scene for uam introduction," *Journal of Air Transport Management*, vol. 87, p. 101852, 2020.

[19] K. Ploetner, C. Al Haddad, C. Antoniou, F. Frank, M. Fu, S. Kabel, C. Llorca, R. Moeckel, A. Moreno, A. Pukhova *et al.*, "Long-term application potential of urban air mobility complementing public transport: an upper bavaria example," *CEAS Aeronautical Journal*, pp. 1–17, 2020.

[20] T. Lombaerts, J. Kaneshige, S. Schuet, G. Hardy, B. L. Aponso, and K. H. Shish, "Nonlinear dynamic inversion based attitude control for a hovering quad tiltrotor evtol vehicle," in *AIAA Scitech 2019 Forum*, 2019, p. 0134.

[21] T. Lombaerts, J. Kaneshige, S. Schuet, B. L. Aponso, K. H. Shish, and G. Hardy, "Dynamic inversion based full envelope flight control for an evtol vehicle using a unified framework," in *AIAA Scitech 2020 Forum*, 2020, p. 1619.

[22] T. A. Johansen and T. I. Fossen, "Control allocation—a survey," *Automatica*, vol. 49, no. 5, pp. 1087–1103, 2013.

[23] W. Durham, K. A. Bordignon, and R. Beck, *Aircraft control allocation*. John Wiley & Sons, 2017.

[24] C. M. H. Tan, "Multidisciplinary modeling & simulation framework for electric vertical take-off & landing (evtol) vehicles," 2020.

[25] "The vertical flight society. vertical flight society announces continued strong growth," https://vtol.org/files/dmfile/vfspressrelease-2020growth_200113.pdf, [Accessed: 2020-10-30].

[26] "A^3 by Airbus. A^3 Vahana," https://acubed.airbus.com, [Accessed: 2020-10-30].

[27] R. Paul and A. Gopalarathnam, "Simulation of flight dynamics with an improved post-stall aerodynamics model," in *AIAA atmospheric flight mechanics conference*, 2012, p. 4956.

[28] B. L. Stevens, F. L. Lewis, and E. N. Johnson, *Aircraft control and simulation: dynamics, controls design, and autonomous systems*. John Wiley & Sons, 2015.

[29] W. Durham, *Aircraft flight dynamics and control*. John Wiley & Sons, 2013.

Control of an eVTOL using nonlinear dynamic inversion

Enenakpogbe, Emmanuel

2022-05-27

Enenakpogbe E, Whidborne JF, Lu L. (2022) Control of an eVTOL using nonlinear dynamic inversion. In: 13th UK Automatic Control Council (UKACC) International Conference (CONTROL2022), 20-22 April 2022, Plymouth, UK

https://doi.org/10.1109/Control55989.2022.9781449